Pore-Network Connectivity and Molecular Sieving of Normal and Isoalkanes in the Mesoporous Silica SBA-2

ARTICLE *in* THE JOURNAL OF PHYSICAL CHEMISTRY C · MAY 2014

Impact Factor: 4.77 · DOI: 10.1021/jp502390p

THE JOURNAL OF PHYSICAL CHEMISTRY C

Article

pubs.acs.org/JPCC

Pore-Network Connectivity and Molecular Sieving of Normal and Isoalkanes in the Mesoporous Silica SBA-2

Manuel Pérez-Mendoza,*[,†] Jorge González,[§,∥] Carlos A. Ferreiro-Rangel,[‡] Magdalena M. Lozinska,[§] David Fairén-Jiménez,[‡] Tina Düren,[‡] Paul A. Wright,[§] and Nigel A. Seaton[‡]

[†]Departamento de Química Inorgánica, Facultad de Ciencias, Universidad de Granada, 18071 Granada, Spain

[‡]Institute for Materials and Processes, School of Engineering, The University of Edinburgh, King's Buildings, Edinburgh EH9 3JL, U.K.

[§]EaStCHEM School of Chemistry, University of St Andrews, North Haugh, St Andrews, Fife KY16 9ST, U.K.

[∥]Facultad de Ciencias Químicas, Universidad de Colima, Colima 28040, México

Supporting Information

ABSTRACT: We have studied the adsorption of *n*-butane and isobutane in the mesoporous silica SBA-2. Our work has two purposes: (i) to better understand the structure of the material, and in particular the impact of calcination on the evolution of the pore network, and (ii) to investigate our ability to tune the structure of SBA-2 to separate normal and isoalkanes by molecular sieving. By a combination of experimental adsorption measurements, molecular simulation, and percolation analysis, we determined the evolution of the sizes of the pores and the connectivity of the pore network as the calcination temperature increases. For a certain range of calcination temperatures, the pore network drops below its percolation threshold for isobutane, while allowing the percolation of *n*-butane, giving an extremely high selectivity for *n*-butane over isobutane. This suggests that tuning the window size of SBA-2 and other structured mesoporous materials of this general type has the potential to generate optimized adsorbents for particular applications.

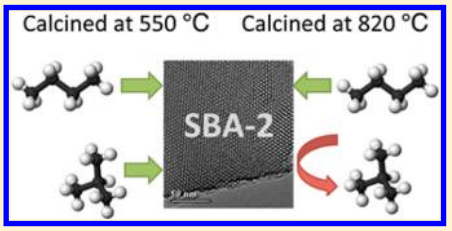

1. INTRODUCTION

Since their discovery in the early 1990s,[1,2] periodic mesoporous silicas (PMSs) have become one of the most versatile families of materials with applications in, for example, gas separation, adsorption, controlled drug release, shape-selective catalytic processes, and sensing.[3−5] The way they are synthesized, using a precursor solution with a silica source and a liquid-crystal phase formed by a surfactant which serves as a template for the porous material, followed by the calcination of the resultant silica network, is the origin of their versatility.[1,2,6] First, the template generates a well-defined long-range order in the structure, while at an atomic level the material is noncrystalline. The use of different precursor solutions and reaction conditions leads to different structures and PMSs exist with mono-, bi-, or tridimensional pore networks and with a wide range of pore sizes.[7−9] The pore size and connectivity of the network affect the equilibrium and dynamics of molecular processes occurring within the pore space such as the adsorption and diffusion of gases. Second, the surface chemistry of the pores can be modified by lining with organic groups and metals either by in-situ co-condensation or by postsynthesis grafting,[10,11] changing for example the hydrophilicity and acidity of the materials, with all the implications this has for their possible uses in selective adsorption and catalysis.

SBA-2 is a PMS with a three-dimensional pore network.[12,13] One of the distinctive features of SBA-2 is that the topology of the network is formed by spherical cavities arranged in either hexagonal close-packed (hcp) or cubic close-packed (ccp) networks, with diameters in the mesopore size range that are interconnected by smaller, cylindrical channels, with sizes in the micropore size range.[12−14] (The ccp material is strictly designated STAC-1, but in this paper we use for convenience the term SBA-2 to refer to both materials. In practice, samples typically contain materials with both structures, intergrown, although recently both pure ccp and pure hexagonal close packed structures have been prepared using a costructure directing agent and gemini surfactant under closely controlled conditions.[15,16]) Thus, the pore structure combines the large volume associated with the cagelike pores with the selectivity with respect to molecular size and shape of the narrow microporous channels. This combination is attractive for applications such as adsorptive separations and shape-selective catalysis.

The channels appear to originate in the close proximity of the spherical micelles during the synthesis process, leading to a concentration of water molecules at the interface and a corresponding tendency for the silica condensation in this region to be relatively slight.[17] We have also suggested that the channels might be further developed when the synthesized material is calcined to remove the surfactant.[18] It is thus

Received: March 9, 2014
Revised: April 25, 2014
Published: April 28, 2014

unlikely that the cages will be connected following a completely regular pattern and that all the channels will have the same size. It is more likely that the calcination process will have an important effect on how these channels are formed and, hence, on the connectivity of the porous network—that is, on the number and size of the channels connecting the cavities. As the connectivity has a direct effect on the accessibility of adsorptives to the pores, this will condition the performance of SBA-2 material as an adsorbent or catalyst support. Therefore, establishing and controlling the relationship between preparation and performance is crucial from the materials design point of view.

In a previous communication,[14] we showed that a model based on a pore size distribution (PSD) of cylinders (representing the interconnecting channels) and spheres (representing the spherical cavities) is able to describe and accurately predict the adsorption of methane and ethane on SBA-2 using the grand canonical Monte Carlo (GCMC) simulation method. In a subsequent paper,[18] we showed that percolation theory, together with the PSD analysis, can be used to understand the accessibility of the pore network to molecules of different sizes and shapes and hence to evaluate the connectivity of the network. The results indicated a much lower effective coordination number for the cavities than expected from the geometric structure of the system. The network was sufficiently well connected that it was above the percolation threshold for both species studied, nitrogen and ethane. That is, both species could gain access to all macroscopic regions of the material, though not necessary to every individual cavity. The effective coordination numbers experienced by the two species were very different, however: 4.9 for nitrogen and 1.8 for ethane. (The value for ethane is just above the percolation threshold for the SBA-2 network, which percolates when the effective coordination number is 1.44.[19])

The purpose of the present work is to improve our understanding of the pore structure of SBA-2 by applying the adsorption−percolation analysis to larger adsorptives with different shapes, *n*-butane (C4) and isobutane (isoC4), and to use this analysis to understand the relationship between the temperature of calcination and the pore structure. This is important for two reasons. First, by using larger molecules than in our earlier study,[18] we gain further insights into the effect of the manufacturing process on the pore structure of SBA-2. Second, we are interested in the potential of SBA-2 for shape-selective adsorption in applications in which a high adsorption capacity is important. The C4/isoC4 system is an example of an important class of industrial processes in which normal and isoalkanes are separated.

2. EXPERIMENTAL SECTION

The SBA-2 samples were prepared at room temperature and alkaline pH using a gemini quaternary ammonium surfactant as template. A complete description of the preparation methodology has been previously reported.[12] Different batches calcined at 700, 800, and 900 °C were prepared to study the influence of calcination temperature in the structure. A solvent-extracted sample (with no calcination) was also prepared. Further samples calcined at 550 and 820 °C were prepared for the study of mixture adsorption.

Powder X-ray diffraction patterns were collected in transmission mode in the form of powder supported in 0.7 mm quartz glass capillaries. Measurements were made at ambient temperature using monochromated Cu $K\alpha_1$ radiation, λ = 1.540 56 Å, on a STOE Stadi/p diffractometer.

Transmission electron microscopy (TEM) micrographs were taken using a JEOL-JEM 2011 electron microscope equipped with a CCD Gatan digital camera operating at 200 keV. Samples were ground before being dispersed in acetone then deposited onto a holey carbon film, supported on a Cu grid.

The adsorption of nitrogen at 77 K and C4 and isoC4 at 268 K was measured from 0 to 1 bar using a Hiden IGA automated gravimetric analyzer. Typically 10−25 mg of sample was used in the determination of each isotherm. Samples were degassed at 383 K for 3 h under vacuum and cooled to room temperature before the dry mass was set. For nitrogen the sample chamber was immersed in liquid nitrogen, whereas for the butanes the temperature of the sample chamber was regulated by a Grants Optima GR150 thermostatic recirculating water bath.

Mixture adsorption experiments were carried out on a bench-scale open-flow adsorption/desorption system. The system has been described previously.[20] In essence, a mixture of a constant composition is allowed to flow past the sample until the outlet composition of the gas reaches steady state, at which point adsorption equilibrium is judged to have been attained. The adsorbed phase is then desorbed by heating to 423 K and collected in a container cooled to 77 K. The amount and composition of the adsorbate are then measured. In these experiments, a 1:1 C4/isoC4 gas mixture was allowed to flow past the sample at 268 K and 0.8 bar.

3. ADSORPTION−PERCOLATION ANALYSIS

The essence of our approach is to treat separately two aspects of adsorption on this material, each of which relates to a different length scale: the local adsorption equilibrium within individual pores and the effect that the pore network has on the accessibility of those pores to different adsorptive species. As in our previous work,[14,18] the channels and cavities in SBA-2 are represented by respectively cylindrical and spherical pores, with the pores having a regular, atomistic surface. The adsorption of a particular species in a particular pore (either a cavity or a channel, with a specified diameter) is modeled using grand canonical Monte Carlo (GCMC) simulation, which generates a local adsorption isotherm, i.e., the equilibrium amount adsorbed as a function of pressure. At this level of the model, the pores are considered to be independent of each other, that is, the fact that in reality the pores are connected together in a network is ignored. A complete description of the GCMC method used can be found in our earlier paper.[14]

It should be noted that a more rigorous treatment of adsorption on SBA-2 would treat the pore network in an integral way, that is, without separately defining cavities and channels as "building blocks" of the network. We have recently published an account of this approach, using a kinetic Monte Carlo (kMC) method to simulate the synthesis of SBA-2 (and the closely related material STAC-1).[17] Using this approach, the connections between the cavities arise naturally from the simulation. Both the individual cavities and the connections between them are rather irregular, while in a statistical sense the cavities remain spherical and their connections have an approximately circular cross section (though their cross-sectional area varies along their axis). The model materials generated by kMC simulation—which we take to be a good representation of the real materials—thus support the use of spherical cavities in the present, simpler model. The representation of the connections generated by kMC

dx.doi.org/10.1021/jp502390p | J. Phys. Chem. C 2014, 118, 10183−10190

simulation as cylinders in the present model is less exact, but the present approach captures the essence of the connections as short, narrow elements with small but finite adsorption capacity. While kMC simulation gives powerful insights into the synthesis and properties of the real materials, the computational demands of that approach are far too great for that method to be used for the extensive adsorption–percolation analysis reported here.

In our simulations, nitrogen was modeled as a two-site Lennard-Jones (LJ) molecule with a quadrupole, following Kjems and Dolling.[21] C4 and isoC4 were modeled as four-site molecules, with the CH_3, CH_2, or CH groups represented by individual LJ sites. The potential parameters are given in Table 1. The silicon atoms are neglected, with their small contribution to the adsorption potential[22] implicitly included in the potential parameters of the oxygen atoms.

Table 1. Potential Parameters for the Fluids and SBA-2

molecule	ε/k_B (K)	σ (Å)	quad moment (C·m^2)	bond length (Å)
N_2 (2 CLJ)[21]	33.4	3.383	−3.712	0.923
$C_4(CH_3)_2$[23]	88.1	3.905		1.53
$C_4(CH_2)_2$[23]	59.4	3.905		1.53
$isoC_4(CH_3)_3$[23]	80.5	3.910		1.53
$isoC_4(CH)$[23]	40.3	3.850		1.53
O	185.0	2.708		

The impact of the pore network on the adsorption—and in particular the effect of constrictions in the network on the accessibility of the pores to different adsorptive species—is modeled using percolation theory. To transform the problem of adsorption on SBA-2 into percolation terms, we note that the accessibility of the network is controlled by the channels ("bonds", in the language of percolation), as the cavities ("sites", in percolation terms) are much larger than both the adsorptive species studied. The channels are of a comparable size to the adsorptive species, so that some permit the passage of both butane isomers (C4 and isoC4), some permit only the passage of the less bulky species (C4), and some permit the passage of neither species. Indeed, our earlier work[18] showed that some channels in SBA-2 are too small even to permit the passage of nitrogen and that some of the channels that would correspond to a fully coordinated network might even be completely absent.

Adsorption on SBA-2 is an example of percolation on a regular lattice. In the simplest form of lattice percolation, the individual elements are either the sites or the bonds. In "site percolation", the network percolates if sufficient sites are occupied so that a connected network of sites spans the material. One then quantifies, for example, the proportion of the sites that are in the percolating cluster of sites—the "accessibility" of the sites. In "bond percolation", the network percolates if sufficient bonds are occupied, and one calculates the accessibility of the bonds. Adsorption in SBA-2 corresponds to a more complex percolation problem in which both sites and bonds must be considered. The bonds determine the accessibility of the network, while both the sites and the bonds contribute to adsorption. In percolation terms, a site or bond is defined to be "occupied" if it is large enough to accommodate the species of interest, so that a percolating cluster of sites and bonds would allow adsorption of that species. In the study of the adsorption of nitrogen, C4, and isoC4 on SBA-2, all the sites are occupied as they are larger than all these species; the site occupation probability, $p^s = 1$. In contrast, only some of the bonds are occupied, i.e., are large enough to allow the passage of the species; the bond occupation probability, $p^b < 1$. Thus, adsorption in the channels corresponds to bond percolation, while adsorption in the cavities corresponds to what is sometimes termed "site percolation in the bond problem".[19] In the latter case, the network elements of fundamental interest are the sites, while their accessibility is controlled by the bonds; in adsorption terms, adsorption in the cavities is controlled by passage of the adsorptive species through the channels.

The network variable that controls the accessibility of both the sites and the bonds (and hence the overall adsorption) is thus the bond occupation probability, p^b. This has a different value, $p^{b,i}$, for each species, *i*. $p^{b,i}$ is related to the mean number of channels per cavity that are large enough to accommodate that species (the "effective" coordination number), z^i, by

$$z^i = Zp^{b,i} \tag{1}$$

where Z is the coordination number of the network; $Z = 12$ for both hcp and ccp networks. The percolation behavior of a network with $Z = 12$ has been computed by Yanuka[19] for both bond percolation and "site percolation in the bond problem". (Yanuka studied only the ccp network. However, as the percolation properties of a network depend mainly on the dimensionality and coordination number, and only to a small extent on other aspects of the topology,[24] Yanuka's results are applicable to both the ccp and hcp forms of the SBA-2 network.)

The first step in the connectivity analysis[18] is to determine the accessibility of the sites to each species. This is done by using the simulated adsorption isotherms to obtain the pore size distribution (PSD) of the cavities. By using nitrogen, C4, and isoC4 in turn, we obtain three different PSDs, each describing the portion of the pore network that is probed by that species. IsoC4 is more bulky than C4, which in turn is more bulky than nitrogen, so the PSDs are expected to show peaks that diminish in magnitude in the order isoC4 > C4 > nitrogen.

We root the present analysis in information about the accessibility of the SBA-2 pore network from our earlier work.[18] In that work, the SBA-2 sample was prepared by postsynthesis calcination at 550 °C. The nitrogen adsorption isotherm of that material is almost identical to that of the solvent-extracted sample in the present work (reflecting the relatively mild effect of calcination at that relatively low temperature, Figure S1). We are thus able to use the bond occupation probability for nitrogen, $p^{b,n} = 0.41$ (corresponding to $z^n = 4.9$), from that study and apply it to the present solvent-extracted sample. Our adsorption–percolation analysis thus measures changes in the connectivity of the pore network of the various calcined samples, as experienced by different species, relative to the datum of nitrogen adsorption in the solvent-extracted sample. The fraction of cavities accessible to species *i*, $P^{s,i}$, is related to the PSD by

$$P^{s,i} = \frac{\int_0^\infty f^i(r)\,\mathrm{d}r}{\int_0^\infty f^n(r)\,\mathrm{d}r} \tag{2}$$

where $f^i(r) = \mathrm{d}N^i/\mathrm{d}r$: N^i is the number of pores, so that $f^i(r)$ is the probability density function for the number of pores as a

dx.doi.org/10.1021/jp502390p | J. Phys. Chem. C 2014, 118, 10183–10190

function of pore radius. $f^{n}(r)$ is the "reference" distribution, measured using the adsorption of nitrogen on the solvent-extracted sample.

The precise definition of the PSD used in eq 2 requires some discussion. The conventional definition of the PSD, and the form that is obtained directly from adsorption measurements, is the distribution of the pore volume, rather than the pore number, as a function of pore radius; for the spherical cavities considered here, $dN^i/dr = 1/r^3\ dV^i/dr$. For a given material, the set of cavities explored by different adsorptive species differ in their connections to other pores, but not—in a statistical sense—in their size. The ratio of the numbers of pores accessible to different species is therefore the same as the ratio of the pore volumes accessible to different species. In such a case, eq 2 could identically be written in terms of dV^i/dr rather than dN^i/dr. Indeed, this approach was taken in our earlier paper.[18] However, when comparisons are being made between different materials—in our case, samples of SBA-2 calcined at different temperatures, or solvent-extracted—the relationship between accessible volume and accessible number of pores is different for different materials. The materials represented by the numerator and the denominator of eq 2 are different, so the fundamentally correct pore number distribution, dN^i/dr, must be used.

The PSD analysis was carried out by solving the adsorption integral equation using the numerical approach of Davies and Seaton.[25] This relates the overall adsorption, as measured in an experiment, to adsorption in individual pores, represented by Monte Carlo simulations of adsorption on cylindrical and spherical model pores of different sizes. In this way, the simulated adsorption isotherm for each size of cylindrical model pore allows us to detect the "signature" of the corresponding size of channel in the adsorption isotherm of the real material and to quantify this through the PSD. In the same way, the simulated isotherms for the spherical model pores allow us to detect the signature of the corresponding size of cavity. As the isotherms for the model pores are generated using Monte Carlo simulation, this approach to obtaining the PSD is entirely consistent with the use of Monte Carlo simulation to predict adsorption in the material.

Once $P^{s,i}$ has been obtained, we use Yanuka's results for site percolation in the bond problem[19] (shown in Figure 1) in the cavities to obtain $p^{b,i}$, which in turn gives the effective coordination number for this species, z^i.

Thus, the problem of characterizing the connectivity of our SBA-2 network is reduced to the determination of the fraction of cavities accessible to the different adsorptive species under study, which in turn requires the determination of the PSD of the portion of the pore network that is probed by those species. In our work, the PSDs of the portions of the network accessible to nitrogen, butane, and isobutane were obtained by analyzing the experimental adsorption isotherms of those species (at 77 K for nitrogen and 268 K for C4 and isoC4).

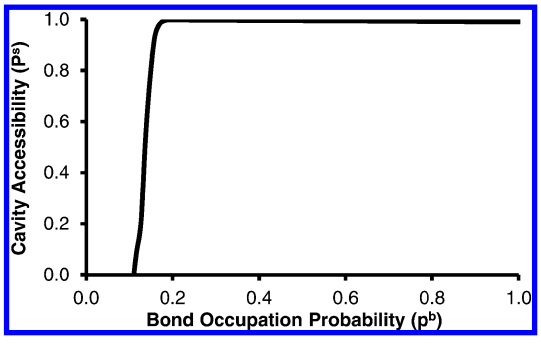

Figure 1. Yanuka's function for site percolation in the bond problem in fcc lattice.[19]

In summary, the steps in the adsorption–percolation analysis of each sample are as follows: (1) For each adsorptive, the PSD is obtained using nitrogen, C4, and isoC4. (2) The PSDs are integrated using eq 2 to obtain $P^{s,i}$. (3) The data of Figure 1 are used to obtain $p^{b,i}$. (4) The effective coordination number experienced by each species is obtained from eq 1.

4. RESULTS AND DISCUSSION

XRD analysis of the samples calcined at different temperatures shows that the symmetry of the network is preserved through the calcination process even for the highest calcination temperature (Figure 2). High-resolution transmission electron

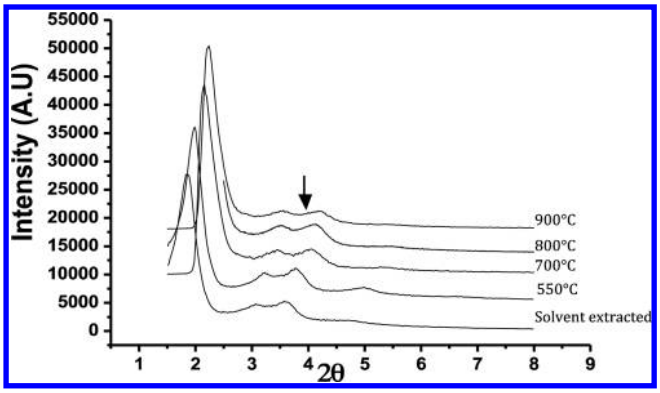

Figure 2. XRD analysis of SBA-2 samples calcined at different temperatures. The solid black arrow indicates the theoretical position of the $(103)_{hex}$ Bragg reflection on the solid calcined at 900 °C.

microscopy confirmed that the ordered close-packed array of cages remained after each calcination.[26] Huo et al.[27] reported that silicate SBA-2 material was thermally stable up to 800 °C. It is clear from our XRD and TEM analysis that the SBA-2 is actually stable up to 900 °C. Nevertheless, the diffraction maxima shift progressively to higher angles with the increase in calcination temperature, indicating a systematic contraction of the unit cell. TEM micrographs of the solids show large cubic domains corresponding to cubic close-packed spherical pores (Figure S2). The absence of any well-defined $(103)_{hex}$ reflection in the XRD patterns, which is expected for the hexagonal close packed array but not for the cubic stacking, also agree with a major proportion of cubic stacking. Indexing the patterns according to the cubic ($Fm\bar{3}m$) structure, the unit cell parameter, a, changes from 81.5 for the extracted sample, to 70 Å for the sample calcined at 900 °C.

The decrease of the a unit-cell parameter is almost linear with the calcination temperature and represents a 35% volume contraction for the sample calcined at the highest temperature. A summary of these data can be found in Table 2. Evidence on the progressive condensation of the amorphous walls of SBA-2 with increasing temperature has also been found by Ferreiro-Rangel et al. using ^{29}Si MAS NMR.[17]

The contraction of the unit cell is also clearly evidenced by the experimental isotherms for the adsorption of nitrogen at 77 K (Figure 3). All these isotherms have two clear steps. The first

dx.doi.org/10.1021/jp502390p | J. Phys. Chem. C 2014, 118, 10183–10190

Table 2. XRD Cell Parameters for the SBA-2 Samples Calcined at Different Temperatures

temperature of calcination (°C)	a (Å)
solvent-extracted	81.5
700	72.8
800	71.6
900	70.0

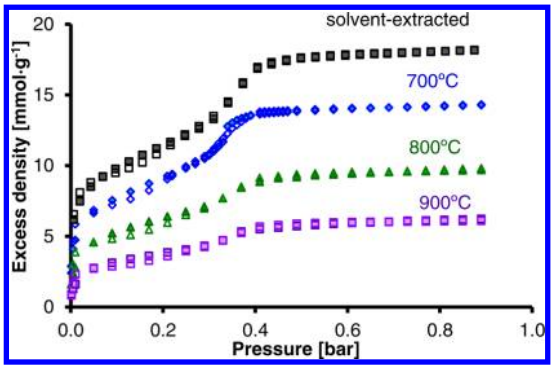

Figure 3. Nitrogen adsorption isotherms at 77 K. Full symbols correspond to experimental results while open symbols represent the predictions from simulation.

occurs at low pressure and is related to adsorption in the regions of the pore space where the adsorption energy is high—that is, in the channels. The second one, at higher pressure, reflects the filling of the cavities by nitrogen; this filling occurs at higher pressure, the larger the cavity. As can be seen in Figure 3, the second step is shifted to lower pressures as we move from the solvent-extracted sample to the three samples calcined at 700, 800, and 900 °C. This shift in the second step indicates a reduction in the mean size of the cavities as the calcination temperature increases, at least up to 700 °C, in broad agreement with the results obtained from the XRD analysis.

There is a progressive decrease in nitrogen adsorption as the calcination temperature increases, although the filling of the cavities takes place at the same pressure. This suggests that the size of the cavities accessible to nitrogen in the samples calcined at 700, 800, and 900 °C is approximately the same, while the number of cavities accessible to nitrogen decreases with the calcination temperature. Thus, the combination of the XRD data and nitrogen adsorption isotherms show that, above a calcination temperature of 700 °C, the main effect of the contraction of the framework is to narrow (or perhaps completely close) at least some of the channels, thereby reducing the accessibility of the cavities to nitrogen.

We now go on to quantify the changing pore structure, already evident from the XRD and nitrogen measurements, using the adsorption–percolation analysis presented in section 3.

The PSD curves for nitrogen adsorption, obtained by analyzing the adsorption data shown in Figure 3, are shown in Figure 4. All the PSDs have two clear maxima: the first is in the microporous region, reflecting adsorption in the channels, and the second is in the mesoporous region, reflecting adsorption in the cavities. These results confirm the conclusions we drew, above, from inspection of the adsorption isotherms themselves.

Compared with the solvent-extracted sample, the sample calcined at 700 °C shows a marked reduction in both the size of

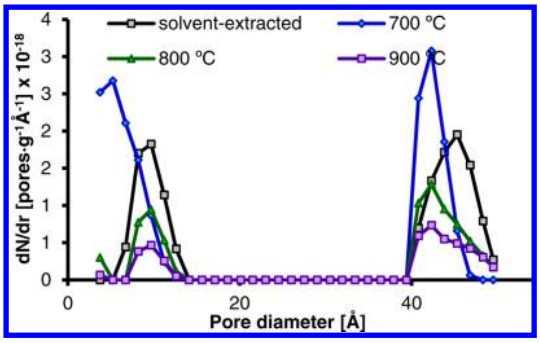

Figure 4. PSDs of SBA-2 samples from nitrogen adsorption at 77 K.

the cavities and the total pore volume. The pore volume accessible to nitrogen decreases further for the samples calcined at 800 and 900 °C while the mean size of the cavities remains constant. This shows that the reduction in the volume accessible to nitrogen for the materials calcined at the higher temperatures is not caused by a reduction in the size of the cavities, but rather in the degree to which the cavities are accessible to nitrogen.

Table 3 shows the results of the adsorption–percolation analysis for the four samples. There is a clear effect of

Table 3. Unit Cell Contraction and Percolation Parameters for Nitrogen Adsorption at 77 K

cal temp (°C)	cell contraction (%)	$P^{s,n}$	$p^{b,n}$	z^n
solvent-extracted[a]	0.0	1.000	0.410	4.90
700	10.7	0.975	0.165	1.98
800	12.1	0.607	0.140	1.68
900	14.1	0.394	0.133	1.59

[a]From ref 12.

calcination at higher temperatures on the accessibility of the cavities to nitrogen. The solvent-extracted sample is the most highly connected, with a value of the bond occupation probability ($p^{b,n}$ = 0.41), and the corresponding effective coordination number (z^n = 4.9, from eq 1), that are so big that essentially all the cavities are accessible to nitrogen ($P^{s,n}$ = 1.0). At 700 °C, the proportion of the cavities that is accessible to nitrogen is only slightly less than unity; $P^{s,n}$ = 0.975. Even this relatively small reduction in the accessibility shows that calcination has caused a substantial reduction in the fraction of the channels that are wide enough to accommodate nitrogen molecules, $p^{b,n}$, which is reduced to 0.165 at 700 °C, with a corresponding reduction in z^n. This reflects the form of Figure 1 in which, far from the percolation threshold, large changes in $p^{b,n}$ (in adsorption terms, the ability of the channels to accommodate the adsorptive species) correspond to small changes in accessibility; this is characteristic of percolation in general. In contrast, as the percolation threshold is closely approached from above, small changes in $p^{b,n}$ lead to the collapse of the accessibility, as we will see below.

As the calcination temperature is increased to 800 and 900 °C, the connectivity of the network progressively decreases, as shown in Table 3. Nevertheless, even for the least well-connected network, that of the sample calcined at 900 °C, the network remains above the percolation threshold for the adsorption of nitrogen; at this temperature, $p^{b,n}$ = 0.133 and z^n = 1.59, whereas the corresponding figures for the percolation threshold are 0.12 and 1.4, respectively.

dx.doi.org/10.1021/jp502390p | J. Phys. Chem. C 2014, 118, 10183–10190

The experimental adsorption isotherms at 268 K for C4 and isoC4 are shown in Figures 5 and 6, respectively. The isotherms for both hydrocarbons show a step corresponding to the filling of the cavities, as for the nitrogen isotherms.

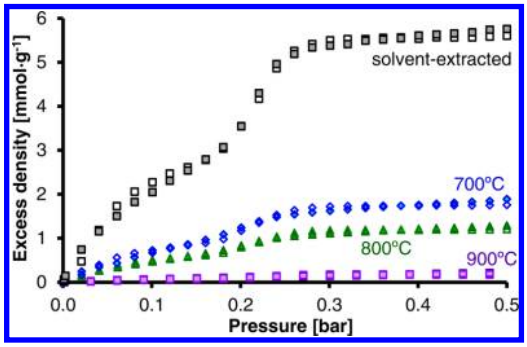

Figure 5. C4 adsorption isotherms at 268 K. Full symbols correspond to experimental results while open symbols represent the predictions from simulation.

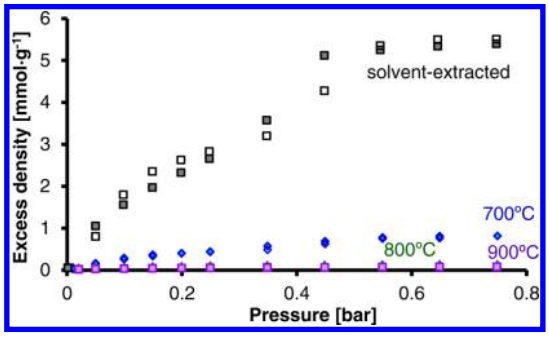

Figure 6. IsoC4 adsorption isotherms at 268 K. Full symbols correspond to experimental results while open symbols represent the predictions from simulation.

The step at low pressure which appeared in the nitrogen isotherms is, however, absent; this reflects the fact that the channels have only a small capacity for the adsorption of larger and more complex C4 and isoC4. It is clear that the dramatic decrease in adsorption capacity for both butane isomers on samples calcined at high temperatures, which is more pronounced than in the case of nitrogen adsorption, cannot be attributed solely to the reduction in unit-cell size. The PSDs are shown in Figures 7 and 8. The adsorption–percolation analysis yields the results shown in Table 4.

It is clear that the solvent-extracted sample is freely accessible to both C4 and isoC4, as it is to nitrogen; the pore structure

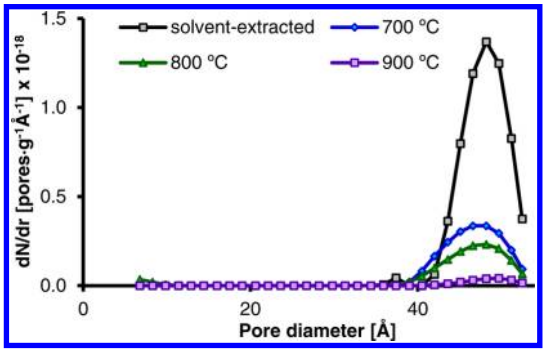

Figure 7. PSDs from C4 adsorption data at 268 K.

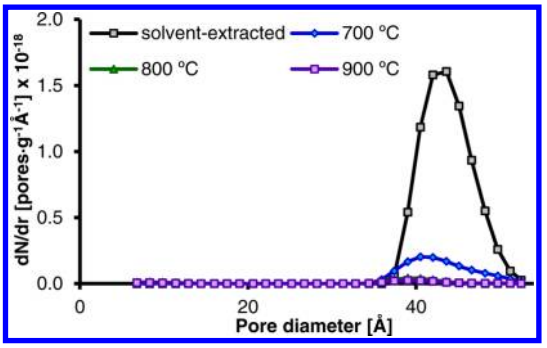

Figure 8. PSDs from isoC4 adsorption data at 268 K.

Table 4. Percolation Parameters for Butane and Isobutane Adsorption at 268 K[a]

	C4			isoC4		
sample	$P^{s,n}$	$p^{b,C4}$	z^{C4}	$P^{s,n}$	$p^{b,isoC4}$	z^{isoC4}
solvent-extracted	0.756	0.147	1.76	0.985	0.170	2.04
700	0.250	0.128	1.54	0.155	0.124	1.49
800	0.168	0.125	1.50	0.023		
900	0.023			0.015		

[a]The absent values indicate that the pore network of the sample is below its percolation threshold so that—beyond noting that point—no connectivity information can be obtained.

does not carry out any sieving of the two butane isomers. Nevertheless, some channels are too small to allow the passage of C4 and isoC4; p^b = 0.147 for C4 and 0.170 for isoC4, in comparison to 0.410 for nitrogen.[18] (The difference in the values of p^b for C4 and isoC4 indicates that the isoC4 can pass through slightly more channels than can the less bulky isomer, C4. While this is, in principle, an anomalous result, the difference is small compared with the difference between the values of p^b for the two butane isomers, on the one hand, and nitrogen, on the other.) As these values for the bond occupation probability are not yet close to the percolation threshold of the network (p^b = 0.12), the constrictions in the pore network do not translate to substantially reduced accessibilities and adsorption capacities. In other words, despite the much smaller number of channels that are large enough to allow the passage of the butane isomers, the subnetwork formed by these channels is still sufficiently highly connected to allow access to almost all the cavities.

The adsorption–percolation analysis of the samples calcined at higher temperature shows a very different picture. As in the case of the nitrogen results, shown in Table 3, Table 4 shows that there is a substantial reduction in the accessibility of the networks at calcination temperatures of 700 °C and above. This reduction in accessibility, calculated using the adsorption–percolation analysis, reflects the changes in adsorption shown in the isotherms of Figures 5 and 6. At a calcination temperature of 700 °C, while adsorption is less than for the solvent-extracted sample, the adsorption of both isomers remains substantial. The percolation data of Table 4 confirm that the network of the sample calcined at 700 °C is accessible to both isomers. At 800 °C, the adsorption of isoC4 is negligible, while there is still substantial (though much reduced) adsorption of C4. At this temperature, the pore network is accessible to C4 but inaccessible to isoC4. Expressed in percolation terms, the percolation threshold of the network is passed at different calcination temperatures for the two species. At 800 °C, the

dx.doi.org/10.1021/jp502390p | J. Phys. Chem. C 2014, 118, 10183–10190

network is still percolating to C4, with 17% of the cavities accessible and an effective coordination number ($z^{b,C4}$ = 1.5) just above the percolation threshold (z^n = 1.4). For isoC4, in contrast, there is very little adsorption and the pore network is below its percolation threshold. At the still higher calcination temperature of 900 °C, Table 4 shows that the pore network of the sample is below the percolation threshold for both butane isomers; the adsorption of both isomers is negligible. In contrast, as we showed above, the pore network remains accessible to nitrogen even at this highest calcination temperature.

This behavior suggests the possibility of using the calcination process to fine-tune the accessibility to the SBA-2 mesoporous structure of different adsorptives, in order to achieve a molecular-sieving effect. For the system we have studied in the present paper, we know that calcination temperatures above about 700 °C give SBA-2 samples that have a substantial capacity for the adsorption of pure C4, and a very low capacity for the adsorption of isoC4, because the latter molecule does not significantly penetrate the pore network. This suggests that, in adsorption from a mixture of these two species, this material should selectively adsorb C4 over isoC4—in other words, it would exhibit molecular sieving of the branched alkane, allowing the linear alkane to adsorb. The separation of normal and isoalkanes is an important industrial adsorption process,[28] and the combination of the high capacity of SBA-2 materials—due to the cavities—and the tunable molecular sieving—due to the channels—is of potential industrial interest. More fundamentally, this would be an illustration of the separation manipulation of pore size and connectivity effects in the design of porous materials. To test our hypothesis, we have carried out mixture adsorption experiments with a mixture of C4 and isoC4, using two samples of SBA-2—one calcined at 550 °C and one at 820 °C. The effectiveness of this separation can be quantified in terms of the selectivity of the material for C4 over isoC4, defined as

$$S = \frac{x/(1-x)}{y/(1-y)} \tag{3}$$

where x and y are the mole fractions of C4 (the more strongly adsorbed species) in the adsorbed phase and in the bulk-gas phase, respectively. On the basis of our observation that the capacity of SBA-2 for isoC4 becomes very small at calcination temperatures above about 700 °C, we would expect the selectivity to be very high for the sample calcined at 820 °C. This is confirmed by the mixture adsorption measurements, in which we found S = 510 for calcination at 820 °C and S = 6.6 for calcination at 550 °C. The latter value reflects the adsorption selectivity of the essentially unconstricted SBA-2 network for C4 over isoC4. It follows, therefore, that the constriction of the pore network caused by calcination at high temperature, leading to the network becoming largely inaccessible to isoC4, increases the selectivity by a factor of about 100.

5. CONCLUSIONS

Our study of the adsorption of nitrogen and the two butane isomers on a series of SBA-2 materials calcined at different temperatures gives a clear picture of changes in the pore structure as the calcination temperature increases. The adsorption−percolation analysis shows that the network becomes increasingly constricted as the calcination temperature increases, reducing the accessibility of the network to all three species studied. The more bulky the molecule, the more susceptible it is to these constrictions. While the SBA-2 pore network remains accessible to nitrogen even at the highest calcination temperature, 900 °C, it becomes inaccessible to isoC4 at a lower calcination temperature than is the case for C4. The long-range order of SBA-2 remains intact even at the highest calcination temperature.

The fact that the two butane isomers have a different percolation threshold, as a function of the calcination temperature, suggests using the calcination temperature as a design parameter, the tuning of which could give an adsorbent with a high selectivity for the C4/isoC4 separation (and, in principle, for other separations of linear and branched hydrocarbons). Our mixture adsorption measurements confirmed that this effect occurs in practice. SBA-2 thus demonstrates an interesting combination of high adsorption capacity, due to the cavities, and a molecular sieving effect, due to the channels connecting the cavities. Furthermore, it should be possible to generalize this approach to tune the window size of mesoporous solids containing cages to optimize molecular selectivity for molecules of sizes extending into the nanometer regime, where the pores of zeolites—conventionally used for molecular-sieving applications—would be too small to allow uptake.

■ ASSOCIATED CONTENT

Supporting Information

Nitrogen adsorption isotherms of SBA-2 solvent-extracted and calcined at 550 °C[16] and TEM micrographs of SBA-2 solid calcined at 900 °C. This material is available free of charge via the Internet at http://pubs.acs.org.

■ AUTHOR INFORMATION

Corresponding Author

*E-mail: mjperezm@ugr.es (M.P.-M.).

Present Addresses

N.A.S.: Abertay University, Dundee DD1 1HG, United Kingdom.

D.F.-J.: Department of Chemical Engineering & Biotechnology, University of Cambridge, Pembroke Street, Cambridge, CB2 3RA, UK.

Notes

The authors declare no competing financial interest.

■ ACKNOWLEDGMENTS

We thank the DeSSANS project (EU FP6 STREP SES6CT2005-020133) and The University of Edinburgh for financial support. J. González also acknowledges financial support from FRABA-Universidad de Colima 761/11.

■ REFERENCES

(1) Kresge, C. T.; Leonowicz, M. E.; Roth, W. J.; Vartuli, J. C.; Beck, J. S. Ordered Mesoporous Molecular-Sieves Synthesized by a Liquid-Crystal Template Mechanism. *Nature* **1992**, *359* (6397), 710−712.

(2) Beck, J. S.; Vartuli, J. C.; Roth, W. J.; Leonowicz, M. E.; Kresge, C. T.; Schmitt, K. D.; Chu, C. T. W.; Olson, D. H.; Sheppard, E. W.; McCullen, S. B.; et al. A New Family of Mesoporous Molecular-Sieves Prepared with Liquid-Crystal Templates. *J. Am. Chem. Soc.* **1992**, *114* (27), 10834−10843.

(3) Ciesla, U.; Schuth, F. Ordered Mesoporous Materials. *Microporous Mesoporous Mater.* **1999**, *27* (2−3), 131−149.

(4) Yiu, H. H. P.; Wright, P. A. Enzymes Supported on Ordered Mesoporous Solids: A Special Case of an Inorganic-Organic Hybrid. *J. Mater. Chem.* **2005**, *15* (35−36), 3690−3700.
(5) Garcia-Bennett, A. E. Synthesis, Toxicology and Potential of Ordered Mesoporous Materials in Nanomedicine. *Nanomedicine* **2011**, *6* (5), 867−877.
(6) Beck, J. S.; Vartuli, J. C.; Kennedy, G. J.; Kresge, C. T.; Roth, W. J.; Schramm, S. E. Molecular or Supramolecular Templating - Defining the Role of Surfactant Chemistry in the Formation of Microporous and Mesoporous Molecular-Sieves. *Chem. Mater.* **1994**, *6* (10), 1816−1821.
(7) Zhao, D. Y.; Huo, Q. S.; Feng, J. L.; Chmelka, B. F.; Stucky, G. D. Nonionic Triblock and Star Diblock Copolymer and Oligomeric Surfactant Syntheses of Highly Ordered, Hydrothermally Stable, Mesoporous Silica Structures. *J. Am. Chem. Soc.* **1998**, *120* (24), 6024−6036.
(8) Van der Voort, P.; Mathieu, M.; Mees, F.; Vansant, E. F. Synthesis of High-Quality MCM-48 and MCM-41 by Means of the Gemini Surfactant Method. *J. Phys. Chem. B* **1998**, *102* (44), 8847−8851.
(9) Tanev, P. T.; Pinnavaia, T. J. A Neutral Templating Route to Mesoporous Molecular-Sieves. *Science* **1995**, *267* (5199), 865−867.
(10) Park, S. S.; Ha, C. S. Organic-Inorganic Hybrid Meseporous Silicas: Functionalization, Pore Size, and Morphology Control. *Chem. Rec.* **2006**, *6* (1), 32−42.
(11) Angloher, S.; Bein, T. *Organic Functionalisation of Mesoporous Silica*; Elsevier Science BV: Amsterdam, 2005; pp 2017−2026.
(12) Hunter, H. M. A.; Garcia-Bennett, A. E.; Shannon, I. J.; Zhou, W. Z.; Wright, P. A. Particle Morphology and Microstructure in the Mesoporous Silicate SBA-2. *J. Mater. Chem.* **2002**, *12* (1), 20−23.
(13) Zhou, W. Z.; Hunter, H. M. A.; Wright, P. A.; Ge, Q. F.; Thomas, J. M. Imaging the Pore Structure and Polytypic Intergrowths in Mesoporous Silica. *J. Phys. Chem. B* **1998**, *102* (36), 6933−6936.
(14) Perez-Mendoza, M.; Gonzalez, J.; Wright, P. A.; Seaton, N. A. Elucidation of the Pore Structure of SBA-2 Using Monte Carlo Simulation to Interpret Experimental Data for the Adsorption of Light Hydrocarbons. *Langmuir* **2004**, *20* (18), 7653−7658.
(15) Han, L.; Sakamoto, Y.; Terasaki, O.; Li, Y.; Che, S. Synthesis of Carboxylic Group Functionalized Mesoporous Silicas (Cfmss) with Various Structures. *J. Mater. Chem.* **2007**, *17* (12), 1216−1221.
(16) Ma, Y. H.; Han, L.; Miyasaka, K.; Oleynikov, P.; Che, S. N.; Terasaki, O. Structural Study of Hexagonal Close-Packed Silica Mesoporous Crystal. *Chem. Mater.* **2013**, *25* (10), 2184−2191.
(17) Ferreiro-Rangel, C. A.; Lozinska, M. M.; Wright, P. A.; Seaton, N. A.; Duren, T. Kinetic Monte Carlo Simulation of the Synthesis of Periodic Mesoporous Silicas SBA-2 and STAC-1: Generation of Realistic Atomistic Models. *J. Phys. Chem. C* **2012**, *116* (39), 20966−20974.
(18) Perez-Mendoza, M.; Gonzalez, J.; Wright, P. A.; Seaton, N. A. Structure of the Mesoporous Silica SBA-2, Determined by a Percolation Analysis of Adsorption. *Langmuir* **2004**, *20* (22), 9856−9860.
(19) Yanuka, M. *Percolation Theory and Capilarity in Relation to Pore Geometry*; University of Guelph: Guelph, 1984.
(20) Yun, J. H.; Duren, T.; Keil, F. J.; Seaton, N. A. Adsorption of Methane, Ethane, and Their Binary Mixtures on MCM-41: Experimental Evaluation of Methods for the Prediction of Adsorption Equilibrium. *Langmuir* **2002**, *18* (7), 2693−2701.
(21) Kjems, J. K.; Dolling, G. Crystal Dynamics of Nitrogen - Cubic Alpha-Phase. *Phys. Rev. B* **1975**, *11* (4), 1639−1647.
(22) Bezus, A. G.; Kiselev, A. V.; Lopatkin, A. A.; Du, P. Q. Molecular Statistical Calculation of Thermodynamic Adsorption Characteristics of Zeolites Using Atom-Atom Approximation. 1. Adsorption of Methane by Zeolite Nax. *J. Chem. Soc., Faraday Trans.* **1978**, *74*, 367−379.
(23) Jorgensen, W. L.; Madura, J. D.; Swenson, C. J. Optimized Intermolecular Potential Functions for Liquid Hydrocarbons. *J. Am. Chem. Soc.* **1984**, *106* (22), 6638−6646.
(24) Lorenz, C. D.; May, R.; Ziff, R. M. Similarity of Percolation Thresholds on the HCP and FCC Lattices. *J. Stat. Phys.* **2000**, *98* (3−4), 961−970.
(25) Davies, G. M.; Seaton, N. A.; Vassiliadis, V. S. Calculation of Pore Size Distributions of Activated Carbons from Adsorption Isotherms. *Langmuir* **1999**, *15* (23), 8235−8245.
(26) Gonzalez, J. PhD Thesis, University of St Andrews, 2005.
(27) Huo, Q. S.; Leon, R.; Petroff, P. M.; Stucky, G. D. Mesostructure Design with Gemini Surfactants - Supercage Formation in a 3-Dimensional Hexagonal Array. *Science* **1995**, *268* (5215), 1324−1327.
(28) Yang, R. T. *Gas Separation by Adsorption Processes*; Imperial College Press: London, 1987.